g-mode oscillations in neutron stars with hyperons

Vinh Tran [1,*] Suprovo Ghosh [2,†] Nicholas Lozano [1,‡] Debarati Chatterjee [2,§] and Prashanth Jaikumar [1,‖]
[1]*Department of Physics and Astronomy, California State University Long Beach, Long Beach, California 90840, USA*
[2]*Inter-University Centre for Astronomy and Astrophysics, Pune University Campus, Pune 411007, India*

(Received 6 January 2023; accepted 22 June 2023; published 14 July 2023)

A common alternative to the standard assumption of nucleonic composition of matter in the interior of a neutron star is to include strange baryons, particularly hyperons. Any change in composition of the neutron star core has an effect on *g*-mode oscillations of neutron stars, through the compositional dependence of the equilibrium and adiabatic sound speeds. We study the core *g* modes of a neutron star containing hyperons, using a variety of relativistic mean field models of dense matter that satisfy observational constraints on global properties of neutron stars. Our selected models predict a sharp rise in the *g*-mode frequencies upon the onset of strange baryons. Should *g* modes be observed in the near future, their frequency could be used to test the presence of hyperonic matter in the core of neutron stars.

DOI: 10.1103/PhysRevC.108.015803

I. INTRODUCTION

The composition of matter in the interior of a neutron star, uncertain at present, is relevant to fundamental questions about the phase of strongly interacting, cold and dense matter [1–3]. An equation of state, which relates state variables in thermodynamic equilibrium, may be derived from a theoretical model of purely nucleonic matter (npe or $npe\mu$) [4–6], hyperonic matter ($npe\mu Y$) [5–10], matter with Bose condensates or delta baryons [5,11], or hybrid matter with a phase transition from nucleonic to quark degrees of freedom [1,6,10], to name a few possibilities. One way to test various theoretical models of dense matter is to compare predicted macroscopic properties of neutron stars (NSs) with astronomical observations. For example, the appearance of hyperons can alter a neutron star's maximum mass, radius, cooling, or gravitational wave (GW) emission from unstable quasinormal modes compared to the purely nucleonic scenario [12].

Theoretical models of neutron stars must satisfy maximum mass constraints gleaned from, e.g., observations of the "black widow" pulsar PSR J0952-0607, the heaviest neutron star to date with mass of $2.35^{+0.17}_{-0.17}\,M_\odot$ [13], or the suggested secondary component in the binary merger event GW190814 [14] with mass of $2.5M_\odot$ or higher. The so-called "hyperon puzzle" refers to the softening effect of hyperons that makes such constraints hard or impossible to satisfy [15], though many solutions have been proposed [9,16,17]. Recent observational constraints from the Neutron star Interior Composition Explorer collaboration (NICER) indicate a mass of $1.34^{+0.15}_{-0.16}\,M_\odot$ and radius of $12.71^{+1.14}_{-1.19}$ km from [18], and [19] reports $1.44^{+0.15}_{-0.14}\,M_\odot$ and radius of $13.02^{+1.24}_{-1.06}$ km for the same star. Similarly, NICER observations of PSR J0740 + 6620 yield a mass of $2.08^{+0.08}_{-0.07}\,M_\odot$ with equatorial radius of $13.7^{+2.6}_{-1.5}$ km from [20] and $2.072^{+0.067}_{-0.066}\,M_\odot$ with radius $12.39^{+1.30}_{-0.98}$ km from [21]. Gravitational wave observations from compact binary merger events such as GW170817 [22] and GW190814 [14] are another probe of the equation of state [23]. Assuming that the secondary object in GW190814 is a heavy neutron star, the analysis in [14] yields the tidal deformability $\Lambda_{1.4}$ of a canonical mass neutron star to be 616^{+273}_{-158}.

While these constraints are narrowing the allowed range of neutron star mass and radius, it is difficult to draw firm conclusions on, or distinguish between, different interior compositions based on static global properties of neutron stars alone [24–26]. Although the presence of non-nucleonic species such as hyperons or phase transitions to quark matter tend to lead to a softening of the equation of state and some tension with astrophysical constraints [12,27–29], there are still many models that satisfy current astrophysical constraints [30–32]. A different approach, namely that of stellar oscillations, may provide a new tool for addressing the problem of composition more directly. The secular quasinormal oscillation modes of neutron star carry information about the interior composition and viscous forces that damp these modes [33–35]. Examples include the fundamental f mode, p modes, and g modes (driven by pressure and buoyancy respectively), as well as r modes (Coriolis force) and pure space-time w modes. Several of these modes may be excited during a supernova explosion, or in isolated perturbed neutron stars, or during the post-merger phase of a binary NS [36–38]. Spin and eccentricity may enhance the excitation of the f modes during the inspiral phase of a neutron star merger [39,40]. The fundamental f modes as well as composition-driven g modes are within the sensitivity range of current generation of GW detectors and the former is correlated with the tidal deformability [41–44].

*vinh.tran02@student.csulb.edu
†suprovoh@iucaa.in
‡Nicholas.lozano@csulb.edu
§debarati@iucaa.in
‖prashanth.jaikumar@csulb.edu

Our focus in this work will be on g modes of hyperonic stars. It is known that g modes are particularly sensitive to composition, as shown in studies ranging from npe and $npe\mu$ matter [25] to hybrid stars exhibiting a first-order phase transition from nucleonic matter to a deconfined quark phase [45] or in a crossover model [31]. It was found that the appearance of quarks in neutron star matter, especially via a first order transition, leads to a dramatic increase in the g-mode oscillation frequency. In this work, we extend this analysis to consider compositions including hyperons as well ($npe\mu Y$).

This paper is organized as follow: In Sec. II we introduce the theoretical framework for g-mode oscillation, followed by a discussion in Sec. III of two sound speeds c_s^2 and c_e^2, whose difference drives the g mode. In Sec. IV, we introduce the relativistic mean field models (RMF) we sample for our calculations: phenomenological models that treat baryons as fundamental fields interacting via mesons [7,46,47]. In Sec. V, we outline the method we use for calculating the adiabatic sound speed via the sound speed difference expression introduced in Sec. III. In Sec. VI we present our results for the g-mode oscillation frequencies, followed by our conclusions in Sec. VII and an instructive derivation on sound speeds in the Appendix A.

II. g-MODE OSCILLATIONS

In the general theory of linearized nonradial oscillations of an ideal self-gravitating fluid composing a compact star, the oscillatory fluid displacement of a mode with quantum numbers nlm is represented by a vector field $\vec{\xi}^{nlm}(\vec{r},t)$, conveniently separable in a spherically symmetric background into radial and tangential components $\xi_r^{nlm}(\vec{r},t)=\eta_r^{nl}(r)Y_{lm}(\theta,\phi)e^{-i\omega t}$ and $\xi_\perp^{nlm}(\vec{r},t)=r\eta_\perp^{nl}(r)\nabla_\perp Y_{lm}(\theta,\phi)e^{-i\omega t}$ respectively, where $Y_{lm}(\theta,\phi)$ are the spherical harmonics. From the perturbed (Newtonian) continuity equation for the fluid, the corresponding pressure perturbation is $\delta p/\rho=\omega^2 r\eta_\perp(r)Y_{lm}(\theta,\phi)e^{-i\omega t}$, where ρ is the energy density. The equations of motion (Euler equation) to be solved to determine the frequency ω_{nl} of a particular nl mode (degenerate in m for nonrotating stars) is

$$\frac{\partial}{\partial r}(r^2\xi_r)=\left[\frac{l(l+1)}{\omega^2}-\frac{r^2}{c_s^2}\right]\left(\frac{\delta p}{\rho}\right), \tag{1}$$

$$\frac{\partial}{\partial r}\left(\frac{\delta p}{\rho}\right)=\frac{\omega^2-N^2}{r^2}(r^2\xi_r)+\frac{N^2}{g}\left(\frac{\delta p}{\rho}\right). \tag{2}$$

where we have suppressed the indices on ω and ξ and $N^2=\frac{c_s^2-c_e^2}{c_s^2c_e^2}$ is the Brunt-Väisälä frequency. Additionally, c_e^2, the equilibrium sound speed, is the total derivative of the pressure p with respect to energy density ε; and c_s^2, the adiabatic sound speed, is the partial derivative of p with respect to ε while holding the composition of matter χ fixed:

$$c_e^2:=\frac{dp}{d\varepsilon},\quad c_s^2:=\left.\frac{\partial p}{\partial\varepsilon}\right|_\chi. \tag{3}$$

As composition of matter is determined by the various particle fractions, holding χ fixed is equivalent to holding all of the independent particle fractions $x_i:=n_i/n_B$ in the system fixed, that is, all the particle fractions except for the electron fraction x_e and the neutron fraction x_n. These latter fractions are instead fixed by constraints of charge neutrality and baryon number conservation.

For a given equation of state (stellar structure), a global solution of the linear perturbation equations, Eqs. (1) and (2), is found to be subject to boundary conditions of regularity at the stellar center ($r\to 0$) and vanishing of the Lagrangian pressure variation[1] $\Delta p=c_s^2\Delta\rho$ at the surface. These solution values represent the discrete g-mode spectrum for a chosen stellar model. As in other works [31,45,48–50], we use the Cowling approximation [51], which neglects the back reaction of the gravitational potential, while extending Eqs. (1) and (2) to include the relativistic effects of the matter [48], which yields

$$-\frac{1}{e^{\lambda/2}r^2}\frac{\partial}{\partial r}[e^{\lambda/2}r^2\xi_r]+\frac{\ell(\ell+1)e^{\nu}}{r^2\omega^2}\frac{\delta p}{p+\varepsilon}-\frac{\Delta p}{\gamma p}=0, \tag{4}$$

$$\frac{\partial\delta p}{\partial r}+g\left(1+\frac{1}{c_s^2}\right)\delta p+e^{\lambda-\nu}h(N^2-\omega^2)\xi_r=0, \tag{5}$$

where N^2, the Brunt-Väisälä frequency, is slightly modified to

$$N^2=g^2\left(\frac{c_s^2-c_e^2}{c_s^2c_e^2}\right)e^{\lambda-\nu}, \tag{6}$$

where $\nu(r)$ and $\lambda(r)$ are metric functions of the unperturbed star which feature in the Schwarzschild *interior* metric, and $\gamma=(n_B/p)\partial p(n_B,Y_p)/\partial n_B$ is the adiabatic index with n_B the baryon density.

The impact of the Cowling approximation, compared to a full general relativistic calculation, typically only affects the frequencies of the g mode at the 5–10% level, and that too only for neutron stars heavier than about $1.6M_\odot$, as shown in [52], therefore it does not change our conclusions qualitatively. Because we have employed the Cowling approximation and ignored the perturbations of the metric that must accompany fluid perturbations, we cannot compute the imaginary part of the eigenfrequency (damping time) of the g mode.[2]

It is useful to precisely define the local and global g modes at the outset. The local g mode refers to the oscillation of a test parcel of fluid located at a distance r from the stellar center, with free boundaries. Equations (1) and (2) can be approximated in the short-wavelength limit ($kr\gg 1$) to show that the local dispersion relation has two distinct branches, with the lower frequency branch corresponding to the frequency of the local g mode. This frequency is then $\omega^2\propto e^{\lambda}N^2$ [50], highlighting the importance of the two sound speeds at any location inside the star [in particular, the difference of their inverse squares, as in Eq. (6)]. On the other hand, the global g mode refers to the motion of all such parcels stitched

[1]The Lagrangian variation of a fluid variable is related to the Eulerian variation through the operator relation $\Delta\equiv\delta+\xi\cdot\nabla$.

[2]The damping time of g modes due to viscosity and gravitational wave emission, estimated in some works [25,53], suggests that the g mode can become secularly unstable for temperatures $10^8<T<10^9$ K for rotational speeds exceeding twice the g-mode frequency of a static star.

together, with boundary conditions imposed at the center and surface of the star. This results in a single eigenvalue for ω which describes the global oscillation of the star of a fixed gravitational mass M and radius R. It can be thought of as an average of the local g modes in the sense that each parcel is sensitive to its local environment only, but the changing profile of that environment from center to surface is taken into account.

In this work, we study the fundamental g mode with $n = 1$ and fix the mode's multipolarity at $l = 2$. This is because the $l = 2$ mode is quadrupolar in nature, and can couple to gravitational waves. Higher l values (octupole and higher) are generally weaker than the quadrupole. The reason to study the $n = 1$ (fundamental) g mode is that the local dispersion relation for g modes $\omega^2 \propto 1/k^2$ implies that the $n = 1$ excitation has the highest frequency, whereas higher values of n are known to have a smaller amplitude of excitation and a weaker tidal coupling coefficient [31]. The frequency of the fundamental g mode is also within the sensitivity range of current generation of gravitational wave (GW) detectors [54,55].

III. SOUND SPEED DIFFERENCE

A necessary quantity for calculating g-mode oscillations is the Brunt-Väisälä frequency, which is proportional to the difference of the squares of two sound speeds, $c_s^2 - c_e^2$, where the equilibrium sound speed c_e^2 is the total derivative of the pressure p with respect to energy density ε and the adiabatic sound speed c_s^2 is the partial derivative of p with respect to ε while holding the composition of the matter χ fixed as defined in Eq. (3). The expressions for p and ε are model dependent, but encapsulate contributions from all particles present.

Starting from the definitions of c_s^2 and c_e^2, the sound speed difference $c_s^2 - c_e^2$ can be written in terms of partial derivatives of specific linear combinations of chemical potentials $\tilde{\mu}_i$ defined in Eqs. (8) and (9) as shown for npe and $npe\mu$ matter in Eqs. (51) and (A34) respectively in [45]. A natural generalization to arbitrary compositions is given in Eq. (7) (as shown in Appendix A):

$$c_s^2 - c_e^2 = \frac{n_B^2}{\mu_n} \sum_i \left.\frac{\partial \tilde{\mu}_i}{\partial n_B}\right|_\chi \frac{dx_i}{dn_B}, \tag{7}$$

where μ_n is the neutron chemical potential, x_i is the particle fraction for the ith independent particle, and $\tilde{\mu}_i$ is a linear combination of chemical potentials satisfying $\tilde{\mu}_i = 0$ in β equilibrium as defined in Eqs. (8) and (9) below. The sum over i accounts for each individual β-equilibrium condition in our system, where in our case $i \in p, \Lambda^0, \Sigma^-, \Sigma^0, \Sigma^+, \Xi^-, \Xi^0$. In essence, Eq. (7) provides a method for calculating the adiabatic sound speed c_s^2 from finding the equilibrium sound speed c_e^2 and sound speed difference $c_s^2 - c_e^2$ separately.

At zero temperature, we have

$$\tilde{\mu}_i = \mu_n - q_i\mu_e - \mu_i, \qquad i \in \text{baryon}, \tag{8}$$

$$\tilde{\mu}_\ell = \mu_e - \mu_\ell, \qquad \ell \in \text{lepton}, \tag{9}$$

where q_i is the charge of the baryon (in units where $q_e = e = 1$) [7] and μ_e is the electron chemical potential. For the baryon octet, the various $\tilde{\mu}_i$ are explicitly given by

$$\tilde{\mu}_p = \mu_n - \mu_e - \mu_p, \quad \tilde{\mu}_{\Lambda^0} = \mu_n - \mu_{\Lambda^0}, \tag{10}$$

$$\tilde{\mu}_{\Sigma^0} = \mu_n - \mu_{\Sigma^0}, \quad \tilde{\mu}_{\Xi^0} = \mu_n - \mu_{\Xi^0}, \tag{11}$$

$$\tilde{\mu}_{\Sigma^-} = \mu_n + \mu_e - \mu_{\Sigma^-}, \quad \tilde{\mu}_{\Xi^-} = \mu_n + \mu_e - \mu_{\Xi^-}, \tag{12}$$

$$\tilde{\mu}_{\Sigma^+} = \mu_n - \mu_e - \mu_{\Sigma^+}, \tag{13}$$

and for the muon $\tilde{\mu}_\mu = \mu_e - \mu_\mu$. Physically, the sound speed difference is a quantitative measure of the restoration of chemical equilibrium when a perturbation occurs. As the g-mode frequency is dependent on $c_s^2 - c_e^2$, it follows that if dx_i/dn_B is large, i.e., when new species enter the system, the g-mode frequency will change sharply. Indeed, that is what we find in our models, as elaborated below.

IV. MODEL FOR NEUTRON STAR STRUCTURE

To model the matter in the core of the star, we use relativistic mean field (RMF) models [7,46,56,57], which are particularly well suited for calculating the adiabatic sound speed via the method described in Sec. III. Specifically, we sample six different RMF models with a variety of different baryon-meson and meson-meson interactions. Four of these are nonlinear relativistic mean field (NLRMF) models: GM1-Y5 [8,58], Big Apple [59,60], and Hornick 65, 70 [61]. The remaining two are density dependent relativistic mean field models (DDRMF): DD-MEX [4,5,9,62] and DD-ME2 [4,5,9,63]. For the most part, these models were originally formulated and provided to model $npe\mu$ matter. We extend these models to include hyperons via a standard SU(6) symmetry argument and fits to hyperonic optical potentials to generate the meson coupling constants. [5,58,64,65].

The equations of motion from the model's Lagrangian, subject to local (charge neutrality) and global conservation laws (baryon number conservation) can be solved for any desired baryon/meson field as a function of baryon density n_B and compositions χ, which then allows for calculating chemical potential derivatives. β equilibrium is then imposed to determine all particle fractions as a function of n_B only.

A. Nonlinear relativistic mean field models

The first class of models that we consider are nonlinear relativistic mean field (NLRMF) models that describe baryon-meson interactions with various mesons such as the isoscalar-scalar σ, isoscalar-vector ω, isovector-vector ρ. Models that include hyperons can also include other strange meson degrees of freedom: the hidden strangeness isoscalar-vector ϕ, the isovector-vector δ, and/or the isoscalar-scalar ξ mesons [9]. Specifically, the NLRMF models we use in this work are Big Apple [59] and Hornick 65 and 70 models [61], with the various baryon-meson and meson-meson coupling constants listed in Table I. These models chosen differ from one another primarily in their baryon-meson and meson-meson interactions. However, as shown in Figs. 4 and 5, neutron stars described by any of these models satisfy current astrophysical constraints on mass, radius and tidal

TABLE I. The parameters of the nonlinear RMF models that we consider in this work including saturation densities n_0, σ meson mass values, and the various coupling constants. The GM1-Y5 model includes the hidden strangeness isoscalar-scalar ξ meson and includes σ self-interactions [8,58]. The Hornick 65 and 70 models include an additional $\omega^2\rho^2$ interaction term [61], and the Big Apple model includes the quartic ω^4 self-interaction as well [59,60]. The models chosen sample a wide range of baryon-meson and meson-meson interactions as a result, allowing us to investigate possible $g-$mode dependence on interaction specific terms, but still produce stars that satisfy all current astrophysical constraints.

Model	GM1-Y5	Hornick 65	Hornick 70	Big Apple
m_σ (MeV)	550.0	550.0	550.0	492.730
n_0 (fm^{-3})	0.153	0.150	0.150	0.155
b	0.002947	–0.00198839	–0.004315	0.005280
c	–0.001070	–0.0028455	–0.004347	–0.003623
Λ_ω	0.0	0.0295148	0.031432	0.047471
ξ_ω	0.0	0.0	0.0	0.00070
$g_{\sigma N}$	9.57	10.4291	9.84608	9.6699
$g_{\omega N}$	10.61	11.7742	10.7467	12.3116
$g_{\rho N}$	8.20	10.1865	9.9829	14.1618
$g_{\sigma\Lambda}$	5.84	5.898	5.99472	5.7656
$g_{\sigma\Sigma}$	3.87	3.991	3.8988775	4.1314
$g_{\sigma\Xi}$	3.06	2.949	3.10215	2.8556
$g_{\omega\Lambda}$	7.0733	7.849	7.16446	8.2077
$g_{\omega\Sigma}$	7.0733	7.849	7.16446	8.2077
$g_{\omega\Xi}$	3.5366	3.925	3.58223	4.1039
$g_{\rho\Lambda}$	0.0	0.0	0.0	0.0
$g_{\rho\Sigma}$	4.10	10.187	9.9829	28.3235
$g_{\rho\Xi}$	8.20	10.187	9.9829	14.1618
$g_{\phi\Lambda}$	–6.02627	–5.5504	–5.0660	5.8037
$g_{\phi\Sigma}$	–6.02627	–5.5504	–5.0660	5.8037
$g_{\phi\Xi}$	–8.9785	–11.1008	–10.1321	11.6075
$g_{\xi\Lambda}$	1.914	0.0	0.0	0.0
$g_{\xi\Sigma}$	0.0	0.0	0.0	0.0
$g_{\xi\Xi}$	0.0	0.0	0.0	0.0

deformability. As a result, we can investigate possible g-mode dependence on interaction-specific terms.

The specific form of meson-meson interactions may vary from one model to another, but the most general Lagrangian can be split into the following terms:

$$\mathcal{L} = \mathcal{L}_{\rm B}^{\rm kin} + \mathcal{L}_{\ell}^{\rm kin} + \mathcal{L}_{\rm M}^{\rm kin} + \mathcal{L}_{\rm int} - U_{\rm NL}, \tag{14}$$

where $\mathcal{L}_{\rm B}^{\rm kin}$ are the kinetic Lagrangians for the baryon fields,

$$\mathcal{L}_{\rm B}^{\rm kin} = \sum_b \bar{\psi}_b (i\gamma^\mu \partial_\mu)\psi_b, \quad b \in \text{baryons}. \tag{15}$$

where we have moved the bare baryon mass terms m_b into the interacting Lagrangian term $\mathcal{L}_{\rm int}$. Likewise, $\mathcal{L}_{\ell}^{\rm kin}$ is the kinetic Lagrangian for the leptonic fields,

$$\mathcal{L}_{\ell}^{\rm kin} = \sum_k \bar{\psi}_k (i\gamma^\mu \partial_\mu - m_k)\psi_k, \quad k = e^-, \mu^-. \tag{16}$$

Then, the kinetic mesonic Lagrangian explicitly is

$$\begin{aligned}\mathcal{L}_{\rm M}^{\rm kin} =& \tfrac{1}{2}\left(\partial^\mu\sigma\,\partial_\mu\sigma - m_\sigma^2\sigma^2\right) + \tfrac{1}{2}\left(\partial^\mu\boldsymbol{\delta}\partial_\mu\boldsymbol{\delta} - m_\delta^2\boldsymbol{\delta}^2\right)\\ &- \tfrac{1}{4}W^{\mu\nu}W_{\mu\nu} + \tfrac{1}{2}m_\omega^2\omega^\mu\omega_\mu - \tfrac{1}{4}\boldsymbol{R}^{\mu\nu}\boldsymbol{R}_{\mu\nu}\\ &+ \tfrac{1}{2}m_\rho^2\boldsymbol{\rho}^\mu\boldsymbol{\rho}_\mu - \tfrac{1}{4}\Phi^{\mu\nu}\Phi_{\mu\nu} + \tfrac{1}{2}m_\phi^2\phi^\mu\phi_\mu\\ &+ \tfrac{1}{2}(\partial_\mu\xi\,\partial^\mu\xi - m_\xi^2\xi^2)\end{aligned} \tag{17}$$

with $W^{\mu\nu} = \partial^\mu\omega^\nu - \partial^\nu\omega^\mu$ and $\boldsymbol{R}^{\mu\nu} = \partial^\mu\boldsymbol{\rho}^\nu - \partial^\nu\boldsymbol{\rho}^\mu$, $\Phi^{\mu\nu} = \partial^\mu\phi^\nu - \partial^\nu\phi^\mu$. In the mean field approximation, where spatial variations of the meson fields are neglected and the meson fields are replaced by their ground state expectation value [7], $\mathcal{L}_{\rm int}$, which describes the baryon-meson interaction, takes the form

$$\begin{aligned}\mathcal{L}_{\rm int} =& -\sum_i \bar{\psi}_i[\gamma_0(g_{\omega i}\omega + g_{\rho i}I_{3i}\rho + g_{\phi i}\phi)\\ &- (m_i - g_{\sigma i}\sigma - g_{\delta i}I_{3i}\delta - g_{\xi i}\xi)]\psi_i,\end{aligned} \tag{18}$$

where ψ_i and m_i are the ith baryon field and bare mass respectively, the $g_{\alpha i}$ for $\alpha \in \omega, \rho, \phi, \xi$ are the coupling constants coupling baryons to mesons, I_{3i} gives the isospin projection of the ith baryon species, and $\omega, \rho, \phi, \sigma, \delta, \xi$ represent the mean field expectation values of the meson fields. Similarly, $U_{\rm NL}$, which describes the meson-meson interactions, is given by

$$\begin{aligned}U_{\rm NL} =& \tfrac{1}{3}bm_N(g_{\sigma N}\sigma)^3 + \tfrac{1}{4}c(g_{\sigma N}\sigma)^4\\ &- \Lambda_\omega g_{\rho N}^2 g_{\omega N}^2\omega^2\rho^2 - \frac{\xi_\omega}{4!}g_{\omega N}^4\omega^4,\end{aligned} \tag{19}$$

where m_N is the nucleon bare mass and $b, c, \Lambda_\omega, \xi_\omega$ are coupling constants. There are three main interactions of note: a cubic and quartic self-interaction of the σ mesons [7,66], a quartic $\omega^2\rho^2$ interaction between ω and ρ mesons, and a quartic ω^4 self-interaction. For an arbitrary Lagrangian of this form, we can identify the chemical potential of a baryon μ_i from the interaction Lagrangian [7,61,66]:

$$\mu_i^* = E_{F_i}^* = \mu_i - g_{\omega i}\omega - g_{\rho i}I_{3i}\rho - g_{\phi i}\phi, \tag{20}$$

where

$$E_{F_i}^* = \sqrt{k_{F_i}^2 + m_i^{*2}} \tag{21}$$

and where k_{F_i} is the Fermi momenta related to the various fermionic number densities n_i (i.e., the vector number density n_i) by

$$n_i := \langle\psi_i^\dagger\psi_i\rangle = \int_0^{k_{F_i}} \frac{d^3k}{(3\pi^2)} = \frac{k_{F_i}^3}{3\pi^2} \tag{22}$$

and the scalar density n_i^s is given by [7]

$$n_i^s := \langle\bar{\psi}_i\psi_i\rangle = \frac{1}{\pi^2}\int_0^{k_{F_i}} \frac{m_i^*}{E_{F_i}^*}k^2\,dk \tag{23}$$

$$= \frac{m_i^*}{2\pi^2}\left[k_{F_i}E_{F_i}^* - m_i^{*2}\ln\frac{k_{F_i} + E_{F_i}^*}{m_i^*}\right]. \tag{24}$$

To solve a particular model for neutron star matter, i.e., to obtain the particle fractions as a function of baryon density in the star as shown in Fig. 1 for the Big Apple energy density

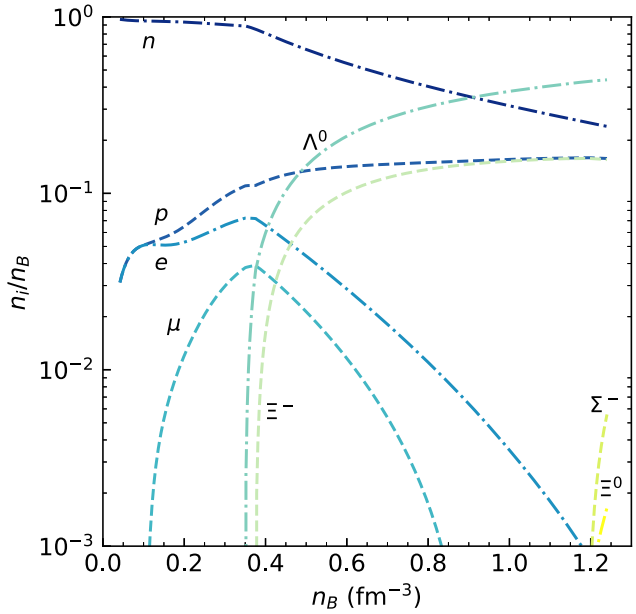

FIG. 1. Particle fractions (n, p, e, μ, Λ^0, Ξ^-, Ξ^0, Σ^-) as a function of total baryon number density n_B for the Big Apple EDF model including hyperons.

functional (EDF) model,[3] we first derived the Euler-Lagrange equations of motion for the mesons from the Lagrangian. Then we applied our constraints of baryon number conservation and charge neutrality,

$$n_B = \sum_i n_i, \qquad i \in \text{baryons}, \tag{25}$$

$$0 = \sum_j q_j n_j, \qquad j \in \text{baryons, leptons}, \tag{26}$$

and imposed chemical equilibrium with respect to weak processes

As a result, for a system of m mesons and n baryons and leptons, we are left with $m+n+1$ unknowns: the m meson field values, the n baryon and lepton fractions, and the total baryon number density n_B. Taking n_B to be our free variable, we solved for the remaining $m+n$ variables at that given value for n_B. One final point to consider is that, for lower values of n_B (which would correspond to the outer layers of the core or lower mass stars), it may not be energetically favorable for heavier particles such as hyperons to appear. Threshold conditions for the emergence of a new particle species are [7]

$$\mu_n - q_b \mu_e \geqslant \mu_b^{(0)}, \tag{27}$$

where

$$\mu_b^{(0)} = m_i^* + \mu_i^{(m)} = m_i^* + g_{\omega i}\omega + g_{\rho i} I_{3i}\rho + g_{\phi i}\phi. \tag{28}$$

Whenever this condition is satisfied, we add the baryon to our system, which involves updating the system of equations.

[3]The particle fractions in the other models are qualitatively similar to the Big Apple EDF results shown in Fig. 1.

From the Lagrangian we can write down the energy momentum tensor [7]

$$\mathcal{T}^{\mu\nu} = \sum_n \frac{\partial \mathcal{L}}{\partial(\partial_\mu \phi_n)} \partial_\nu \phi_n - g_{\mu\nu}\mathcal{L}, \tag{29}$$

which yields the energy density ε and pressure p. In the mean field approximation, the energy density is then

$$\begin{aligned}\varepsilon = {} & \frac{1}{2}m_\sigma^2\sigma^2 + \frac{1}{2}m_\rho^2\rho^2 + \frac{1}{2}m_\phi^2\phi^2 + \frac{1}{2}m_\xi^2\xi^2 + \frac{1}{2}m_\delta^2\delta^2 \\ & + \frac{1}{3}bm_N(g_{\sigma N}\sigma)^3 + \frac{1}{4}c(g_{\sigma N}\sigma)^3 + 3\Lambda_\omega g_{\omega N}^2 g_{\rho N}^2 \omega^2\rho^2 \\ & + \sum_{i\in B}\frac{2J_i+1}{2\pi^2}\int_0^{k_{F_i}}\sqrt{k^2+m_i^{*2}}\,k^2\,dk \\ & + \sum_{\ell}\frac{2J_i+1}{2\pi^2}\int_0^{k_{F_\ell}}\sqrt{k^2+m_i^{*2}}\,k^2\,dk \end{aligned} \tag{30}$$

with the integrals evaluating to

$$\begin{aligned}&\int_0^{k_{F_i}}\sqrt{k^2+m_i^{*2}}\,k^2\,dk \\ &= \frac{1}{4}\left[k_{F_i}\left(k_{F_i}^2+m_i^{*2}\right)^{3/2} + k_{F_i}^3\sqrt{k_{F_i}^2+m_i^{*2}}\right. \\ &\quad \left. - m_i^{*4}\ln\frac{k_{F_i}+\sqrt{k_{F_i}^2+m_i^{*2}}}{m_i^*}\right].\end{aligned} \tag{31}$$

The pressure p follows from the relation [61,64]

$$p = \sum_i \mu_i n_i - \varepsilon \tag{32}$$

With p and ε, we can determine the equilibrium sound speed from

$$c_e^2 := \frac{dp}{d\varepsilon} = \frac{dp}{dn_B}\frac{dn_B}{d\varepsilon} = \frac{dp}{dn_B}\frac{1}{d\varepsilon/dn_B}. \tag{33}$$

Next, we need to consider how to generate the hyperonic coupling constants. Starting with the nucleon-meson couplings that are chosen to satisfy saturation density properties [56,57], we can then generate hyperonic couplings via relationships similar to that expressed in Eq. (34), with the full list of relationships given in [58]:

$$\frac{g_{\omega\Lambda}}{g_{\omega N}} = \frac{1-\frac{2z}{\sqrt{3}}(1-\alpha)\tan\theta}{1-\frac{z}{\sqrt{3}}(1-4\alpha)\tan\theta}. \tag{34}$$

If we take the ideal mixing limit, $\alpha = 1$, $z = 1/\sqrt{6}$, and $\tan\theta = 1/\sqrt{2}$, the relations respect SU(6) symmetry [65,67]:

$$g_{\omega\Lambda} = g_{\omega\Sigma} = 2g_{\omega\Xi} = \frac{2}{3}g_{\omega N}, \tag{35}$$

$$g_{\rho\Lambda} = 0, \quad g_{\rho\Sigma} = 2g_{\omega\Xi} = 2g_{\omega N}, \tag{36}$$

$$g_{\phi N} = 0, \quad 2g_{\phi\Lambda} = 2g_{\phi\Sigma} = g_{\phi\Xi} = \frac{2\sqrt{2}}{3}g_{\omega N}. \tag{37}$$

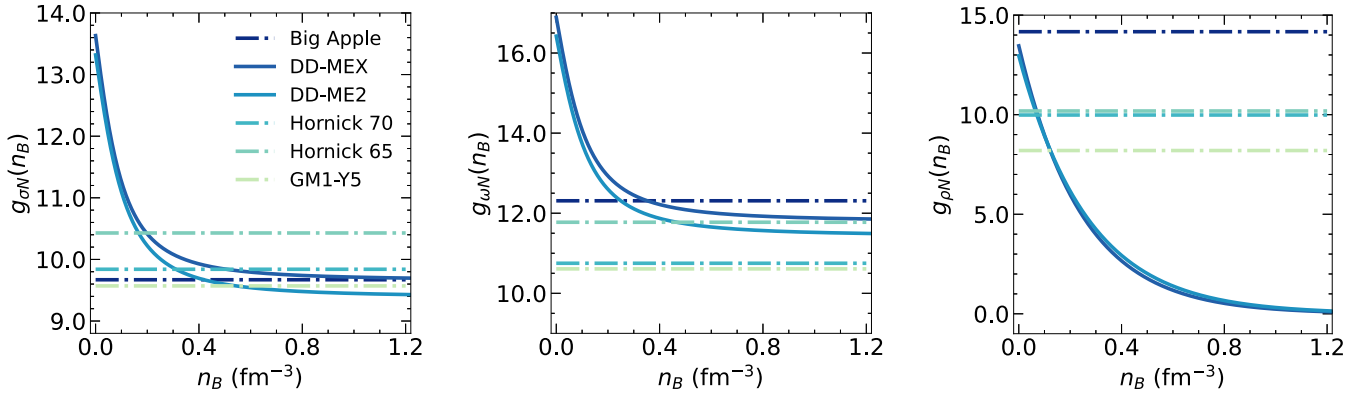

FIG. 2. Density dependence of coupling constants $g_{\sigma N}$, $g_{\omega N}$, and $g_{\rho N}$ for the various DDRMF models. Plotted for reference are the constant coupling constants from the NLRMF models. We see that for large n_B that $g_{\sigma N}$ and $g_{\omega N}$ behave similarly to those in the NLRMF models whereas $g_{\rho N}$ decreases towards zero indicating that in the DDRMF models isospin interactions vanish as $n_B \approx 8n_0$.

For most of our models, we generate the hyperonic-vector meson coupling constants using these SU(6) relations.[4] The coupling constants for scalar fields that couple to mass, that is, the scalar sigma meson, are determined by fitting to hyperonic optical potentials via the following equation [5,65]:

$$U_Y^{(N)} = -g_{\sigma Y}\sigma_0 + g_{\omega Y}\omega_0, \tag{38}$$

where $U_Y^{(N)}$ is the corresponding hyperon optical potential, σ_0 and ω_0 are the saturation density values for the σ and ω mesons, which can be found by solving the standard *npe* case first, and $g_{\omega Y}$ is the omega-hyperon coupling which can be determined using SU(6) relations described previously. For the values of the hyperon potentials at saturation density, we use the most commonly accepted values for $U_\Lambda^{(N)} = -30$ MeV and $U_\Sigma^{(N)} = 30$ MeV [5,9,64,68,69]. Although $U_\Xi^{(N)}$ is known to be attractive, its precise value at saturation is not well constrained [64,68]. For this work, we take it to be $U_\Xi^{(N)} = -14$ MeV in accordance with currently used models [5,9,69]. The hyperonic coupling constants for the strange scalar mesons $g_{\xi Y}$ and $g_{\delta Y}$ can be found by fitting to a more general version of Eq. (38),

$$U_j^{(k)}(n_k) = m_j^* - m_j + \mu_j - \mu_j^*, \tag{39}$$

at densities above saturation when strange degrees of freedom emerge, as a second step after fitting to saturation [58]. However, for the work done here, $g_{\xi Y}$ is only used for GM1-Y5 with values taken as specified in [58], and $g_{\delta Y}$ is not calculated as there is no δ meson dependence in the models that we choose to consider.

B. Density dependent RMF (DDRMF) models

A class of models related to the NLRMF type of models is the density dependent relativistic mean field (DDRMF) model, where the baryon-meson coupling constants are allowed to vary with baryon number density n_B rather than remain constant throughout the entire range of densities. The coupling constants become density dependent and typically take on the forms

$$g_i(n_B) = g_i(n_0)a_i\frac{1 + b_i(n_B/n_0 + d_i)^2}{1 + c_i(n_B/n_0 + d_i)^2} \tag{40}$$

for the σ, ω, ϕ mesons and

$$g_\rho(n_B) = g_\rho(n_0)a_\rho \exp\left[-a_\rho\left(\frac{n_B}{n_0} - 1\right)\right] \tag{41}$$

for the ρ meson, where $g_i(n_0)$ is the coupling constant at saturation and a_i, b_i, c_i, d_i are additional parameters that determine the evolution of the coupling constants for the models [4,5,9,69,70]. The density dependence of a few coupling constants are highlighted in Fig. 2.

There is an additional term added to the chemical potential μ_i called the rearrangement term Σ^r for thermodynamic reasons [5,9,69]:

$$\mu_i^{(b)} = E_{F_i}^* + \mu_i^{(m)} + \Sigma^r(n_B), \tag{42}$$

where for an interaction Lagrangian which includes the scalar-isoscalar σ, vector-isoscalar ω, vector-isovector ρ and hidden-strangeness vector-isoscalar ϕ mesons,

$$\mathcal{L}_{\rm int} = -\sum_i \bar{\psi}_i(\gamma_0\mu_i^* - m_i^*)\psi_i \tag{43}$$

with $\mu_i^* = \mu_i - g_{\omega i}\omega - I_{3i}g_{\rho i}\rho - g_\phi - \Sigma^r$ and $m_i^* = m_i - g_{\sigma i}\sigma$, Σ^r takes the form [4]

$$\Sigma^r(n_B) = \sum_i\Bigg[-\frac{\partial g_\sigma(n_B)}{\partial n_B}\sigma n_i^s + \frac{\partial g_{\omega i}(n_B)}{\partial n_B}\omega n_i + \frac{\partial g_{\rho i}}{\partial n_B}\tau_i^3\rho n_i + \frac{\partial g_{\phi i}}{\partial n_B}\phi n_i\Bigg]. \tag{44}$$

This rearrangement term contributes to the expression for pressure p, though not the energy density ε, which takes on the same form as Eq. (30), which allows us to determine p through the thermodynamic relationship with ε given in Eq. (32).

[4]The GM1-Y5 model takes $z = 0.2$ rather than $z = 1/\sqrt{6}$ [58].

TABLE II. Different DDRMF models chosen for this work and their parameters including saturation density n_0, nonstrange meson coupling constants, and density dependent specific parameters [5,69]. In particular, $g_{\sigma N}(n_0)$, $g_{\omega N}(n_0)$, $g_{\rho N}(n_0)$ refer to the values of the coupling constants at saturation and a_i, b_i, c_i, d_i determine the dependence of the coupling constants on total baryon number density n_B as given by Eqs. (40) and (41).

Model	DD-MEX	DD-ME2
n_0 (fm^{-3})	0.152	0.152
m_σ (MeV)	547.333	550.124
$g_{\sigma N}(n_0)$	10.707	10.540
$g_{\omega N}(n_0)$	13.339	13.019
$g_{\rho N}(n_0)$	7.238	7.367
a_σ	1.397	1.388
b_σ	1.335	1.094
c_σ	2.067	1.706
d_σ	0.402	0.442
a_ω	1.394	1.389
b_ω	1.019	0.924
c_ω	1.606	1.462
d_ω	0.456	0.478
a_ρ	0.620	0.565

To get the hyperon coupling constants, we can employ the same SU(6) symmetry scheme as mentioned in Sec. IV A. The equation relating the hyperon optical potentials to the $g_{\sigma Y}$ coupling constants is modified to include the Σ^r term:

$$U_Y^N = g_{\omega Y}\omega_0 - g_{\sigma Y}\sigma_0 + \Sigma^r(n_B), \tag{45}$$

which for the previously mentioned hyperon optical potentials of $U_\Lambda^N = -30$ MeV, $U_\Sigma^N = 30$ MeV, $U_\Xi^N = -14$ MeV yield the relations $g_{\sigma\Lambda} = 0.6105 g_{\sigma N}$, $g_{\sigma\Sigma} = 0.4426 g_{\sigma N}$, and $g_{\sigma\Xi} = 0.3024 g_{\sigma N}$ [69]. The corresponding hyperon coupling constants are listed in Table III.

TABLE III. Hyperon couplings using SU(6) symmetry arguments as determined by fitting saturation density coupling constants and fields to to Eq. (45) using the following values for the hyperon optical potentials: $U_\Lambda^N = -30$ MeV, $U_\Sigma^N = 30$ MeV, $U_\Xi^N = -14$ MeV [5,9,64,68,69].

Model	DD-MEX	DD-ME2
$g_{\sigma\Lambda}(n_0)$	6.613	6.535
$g_{\omega\Lambda}(n_0)$	8.893	8.679
$g_{\rho\Lambda}(n_0)$	0.0	0.0
$g_{\phi\Lambda}(n_0)$	6.288	6.137
$g_{\sigma\Sigma}(n_0)$	5.0834	4.962
$g_{\omega\Sigma}(n_0)$	8.893	8.679
$g_{\rho\Sigma}(n_0)$	14.476	14.734
$g_{\phi\Sigma}(n_0)$	6.288	6.137
$g_{\sigma\Xi}(n_0)$	3.3319	3.320
$g_{\omega\Xi}(n_0)$	4.446	4.340
$g_{\rho\Xi}(n_0)$	7.238	7.367
$g_{\phi\Xi}(n_0)$	12.576	12.274

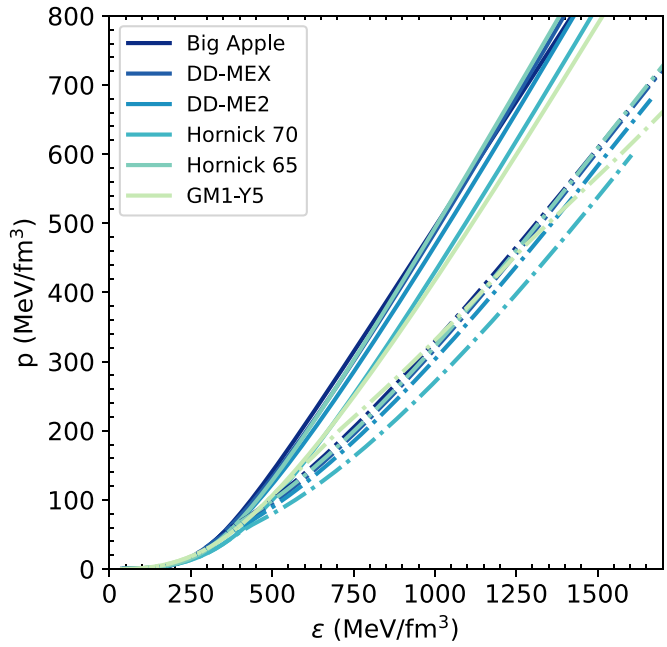

FIG. 3. The equation of state for the various models considered in this work with $npe\mu$ matter (solid line) and $npe\mu Y$ matter (dot-dashed line). The onset of hyperons leads to a characteristic softening of the equation of state [15,29].

Ultimately, we choose the following density dependent RMF models: DD-MEX [62] and DD-ME2 [9], as they produce stars with mass-radius curves and tidal deformabilities in agreement with current astrophysical constraints from NICER and GW170817. Their relevant parameters including coupling constants are listed in Table II. For these models, $U_{\rm NL}$ is effectively zero; that is, there are no nonlinear meson-meson interactions unlike in the nonlinear RMF models. These models are likewise fit to the following saturation parameters: $E_0 = -16.14$ MeV, $K_0 = 267.059$, and 250.89 MeV [5].

C. Equilibrium structure

The pressure p and ε tabulated against total baryon number density give us a parametric equation of state, Fig. 3, which then determines the macroscopic properties such as mass and radius of the star from the Tolman-Oppenheimer-Volkov (TOV) equations (46) and (47) for a static, spherically symmetric star in hydrostatic equilibrium. Figures 4(a), 4(b), and 5 show the corresponding mass-radius plots and tidal deformability with observational constraints (as error bars). The models we use satisfy current observational astrophysical constraints:

$$\frac{dp}{dr} = -\frac{Gm(r)\varepsilon(r)}{r^2}\frac{\left[1+\frac{p(r)}{\varepsilon(r)}\right]\left[1+\frac{4\pi r^3 p(r)}{m(r)}\right]}{1-\frac{2GM(r)}{r}}, \tag{46}$$

$$\frac{dm}{dr} = 4\pi\varepsilon(r)r^2. \tag{47}$$

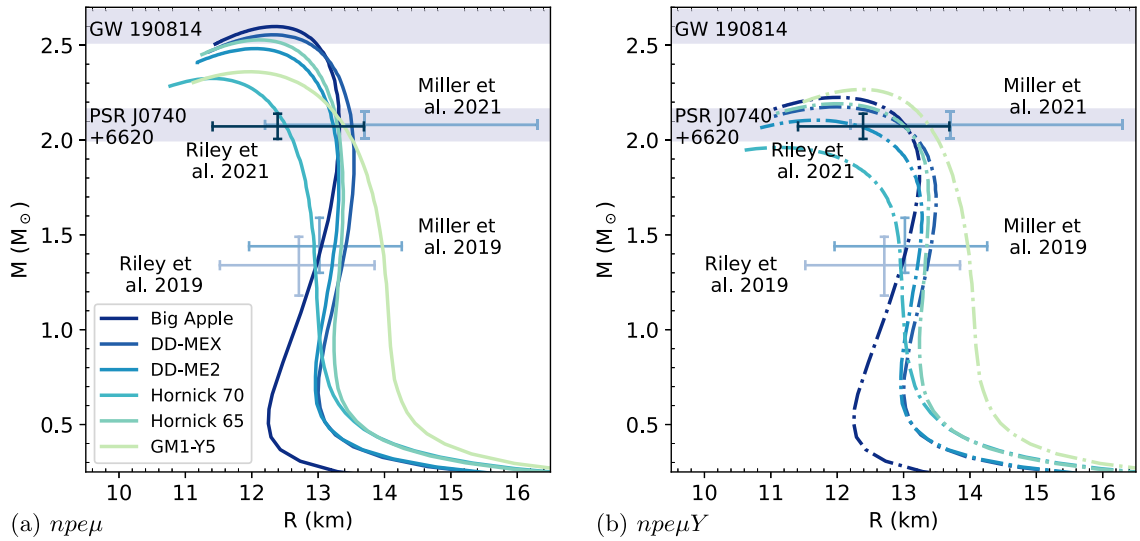

FIG. 4. Mass-radius relations for the various models used in this work with the $npe\mu$ and $npe\mu Y$ compositions on the left and right respectively. The astrophysical constraints of maximum masses from PSR J0740 + 6620 and the secondary object of GW190814 are likewise plotted here in the light blue areas [14,20]. Additionally plotted are the Neutron star Interior Composition Explorer (NICER) constraints on the mass-radius of PSR J0030 + 0451 from Riley *et al.* 2019 ($1.34^{+0.15}_{-0.16}\,M_\odot$ and $12.71^{1.14}_{-1.19}$ km) and Miller *et al.* 2019 ($1.44^{+0.15}_{-0.14}\,M_\odot$ and $13.02^{+1.24}_{-1.06}$ km) [18,19] as well as for PSR J0740 + 6620 with values of ($2.072^{+0.067}_{-0.066}\,M_\odot$ and $12.39^{+1.30}_{-0.98}$ km) and ($2.08^{+0.08}_{-0.07}\,M_\odot$ and $13.7^{+2.6}_{-1.5}$ km) [20,21].

V. ADIABATIC SOUND SPEED VIA SOUND SPEED DIFFERENCE

Having established our working models for the stellar structure and composition, we turn now to the calculation of the adiabatic sound speed squared c_s^2, or equivalently, the sound speed difference (since c_e^2 is easily obtained from the EoS) by using Eq. (7). Starting from Eq.(42), the partial derivative of the baryonic chemical potential[5] is

$$\left.\frac{\partial \mu_i^{(B)}}{\partial n_B}\right|_\chi = \left.\frac{\partial E_{F_i}^*}{\partial n_B}\right|_\chi + \left.\frac{\partial \mu_i^{(m)}}{\partial n_B}\right|_\chi + \left.\frac{\partial \Sigma^r}{\partial n_B}\right|_\chi . \tag{48}$$

We discuss each of these contributions in turn, noting that the effective energy for ith baryon $E_{F_i}^*$ will only couple to the scalar mesons, and $\mu_i^{(m)}$ will only couple to the vector mesons.

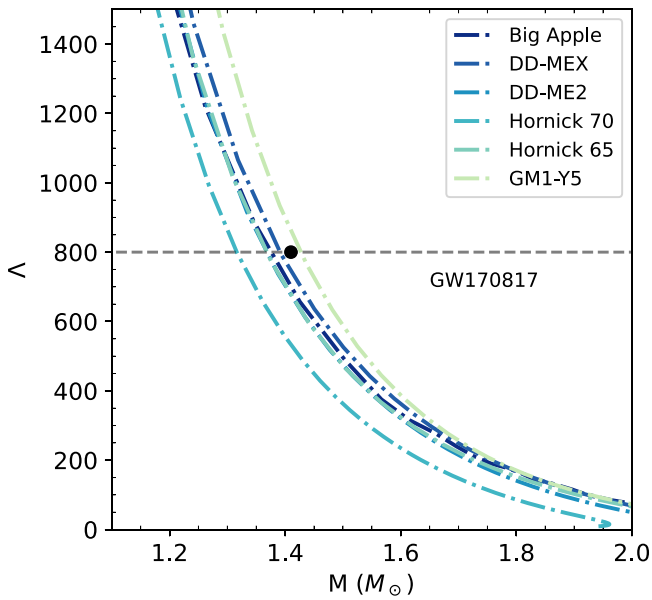

FIG. 5. Tidal deformability plotted against stellar mass for our various models for $npe\mu Y$ compositions. The curves for $npe\mu$ matter are similar. We see that all save for GM1-Y5 are safely below the $\Lambda \leqslant 800$ constraint from GW170817.

A. Partial derivative of the effective energy ($E_{F_i}^*$)

Through Eq. (21), $E_{F_i}^*$ depends on each of the scalar meson fields (say, m in number) σ, δ, ξ through the effective mass term $m_i^* = m_i - g_{\sigma i}\sigma - g_{\xi i}\xi - I_{3i}g_{\delta i}\delta$ for the NLRMF and DDRMF models. To determine $\partial E_{F_i}^*/\partial n_B$, we would need to determine the partial derivatives $\partial\sigma/\partial n_B$, $\partial\xi/\partial n_B$, and $\partial\delta/\partial n_B$ as well. First, for each of the baryons (say, b in number), we have equations for the scalar density given by

$$\begin{aligned} n_i^s = \langle\bar\psi_i\psi_i\rangle &= \frac{1}{\pi^2}\int_0^{k_{F_i}} \frac{m_i^*}{E_{F_i}^*}k^2\,dk \\ &= \frac{m_i^*}{2\pi^2}\left[k_{F_i}E_{F_i}^* - m_i^{*2}\ln\frac{k_{F_i}+E_{F_i}^*}{m_i^*}\right], \end{aligned} \tag{49}$$

providing additional relations between $E_{F_i}^*$ and the meson fields. As a result, after differentiating both sides of Eqs. (21)

[5]The partial derivatives for leptons can be obtained from their relativistic dispersion relation,

$$\left.\frac{\partial \mu_\ell}{\partial n_B}\right|_\chi = \frac{\pi^2 x_\ell}{k_{F_\ell}E_{F_\ell}}, \quad x_\ell := \frac{n_\ell}{n_B}.$$

and Eqs. (B1)–(B6), we arrive at a system of $m+b$ equations that are linear in the quantities of interest, and, in particular, can be solved for $\partial E^*_{F_i}/\partial n_B$. As a concrete illustration, in the NLRMF model, starting with Eq. (21) for $E^*_{F_i}$, we arrive at

$$\left.\frac{\partial E^*_{F_i}}{\partial n_B}\right|_\chi = \frac{\pi^2 x_i}{k_{F_i} E^*_{F_i}} + \frac{m^*_i}{E^*_{F_i}}\left.\frac{\partial m^*_i}{\partial n_B}\right|_\chi, \tag{50}$$

where

$$\left.\frac{\partial m^*_i}{\partial n_B}\right|_\chi = -g_{\sigma i}\left.\frac{\partial \sigma}{\partial n_B}\right|_\chi - g_{\xi i}\left.\frac{\partial \xi}{\partial n_B}\right|_\chi - I_{3i} g_{\delta i}\left.\frac{\partial \delta}{\partial n_B}\right|_\chi. \tag{51}$$

As for each baryon there is an associated $E^*_{F_i}$, each baryon contributes for a total of b equations of this form. Next, from the equation of motion for the the σ meson in particular [Eq. (B1)], after differentiating, we see it likewise depends on $\partial E^*_{F_i}/\partial n_B$ for each baryon through

$$\left.\frac{\partial \sigma}{\partial n_B}\right|_\chi \left(m_\sigma^2 + \frac{\partial^2 U}{\partial \sigma^2}\right) = \sum_j g_{\sigma j}\left.\frac{\partial n^s_j}{\partial n_B}\right|_\chi \tag{52}$$

with $U = \frac{1}{3} b m_N (g_{\sigma N}\sigma)^3 + \frac{1}{4} c (g_{\sigma N}\sigma)^4$ and where

$$\left.\frac{\partial n^s_j}{\partial n_B}\right|_\chi = \frac{\partial}{\partial n_B}\frac{m^*_j}{2\pi^2}\left[k_{F_j}E^*_{F_j} - m^{*2}_j \ln\frac{k_{F_j}+E_{F_j}}{m^*_j}\right], \tag{53}$$

which after expanding, evaluating, and re-inserting into Eq. (52) leads us to Eq. (54), where the relationship between $\partial E^*_{F_i}/\partial n_B$, $\partial\sigma/\partial n_B$, $\partial\xi/\partial n_B$, and $\partial\delta/\partial n_B$ is more explicit.

Similar equations appear when we repeat this procedure for the remaining scalar mesons, contributing a total of m equations to the system. The required derivatives are solved for using standard numerical methods for a linear system of coupled equations:

$$\begin{aligned}
0 = &-\left.\frac{\partial\sigma}{\partial n_B}\right|_\chi\left(m_\sigma^2+\frac{\partial^2 U}{\partial\sigma^2}\right) - \sum_i \frac{g_{\sigma i}}{2\pi^2}\left(g_{\sigma i}\left.\frac{\partial\sigma}{\partial n_B}\right|_\chi + g_{\xi i}\left.\frac{\partial\xi}{\partial n_B}\right|_\chi + I_{3i}g_{\delta i}\left.\frac{\partial\delta}{\partial n_B}\right|_\chi\right)\frac{n^s_i}{m^*_i}\\
&+\sum_i g_{\sigma i}\frac{m^*_i}{2\pi^2}\left[\frac{\pi^2 x_i}{k^2_{F_i}}E^*_{F_i} + k_{F_i}\left.\frac{\partial E^*_{F_i}}{\partial n_B}\right|_\chi\right] + \sum_i g_{\sigma i}\frac{m^*_i}{2\pi^2}\left\{2g_{\sigma i}m^*_i\left(g_{\sigma i}\left.\frac{\partial\sigma}{\partial n_B}\right|_\chi + g_{\xi i}\left.\frac{\partial\xi}{\partial n_B}\right|_\chi + I_{3i}g_{\delta i}\left.\frac{\partial\delta}{\partial n_B}\right|_\chi\right)\ln\frac{k_{F_i}+E^*_{F_i}}{m^*_i}\right.\\
&\left.-m^{*2}_i\left[\frac{\frac{\pi^2 x_i}{k^2_{F_i}}+\left.\frac{\partial E^*_{F_i}}{\partial n_B}\right|_\chi}{k_{F_i}+E^*_{F_i}} + \frac{1}{m^*_i}\left(g_{\sigma i}\left.\frac{\partial\sigma}{\partial n_B}\right|_\chi + g_{\xi i}\left.\frac{\partial\xi}{\partial n_B}\right|_\chi + I_{3i}g_{\delta i}\left.\frac{\partial\delta}{\partial n_B}\right|_\chi\right)\right]\right\}.
\end{aligned} \tag{54}$$

B. Partial derivative of the vector meson contribution to the chemical potential

The contribution of the vector mesons ω, ρ, ϕ to the chemical potential in the mean-field approximation takes the form

$$\mu^{(m)}_i = g_{\omega i}\omega + I_{3i}g_{\rho i}\rho + g_{\phi i}\phi. \tag{55}$$

In a similar fashion to Sec. V A, the partial derivative of $\mu^{(m)}_i$ is dependent on the partial derivatives of the vector meson fields:

$$\left.\frac{\partial\mu^{(m)}_i}{\partial n_B}\right|_\chi = g_{\omega i}\left.\frac{\partial\omega}{\partial n_B}\right|_\chi + I_{3i}g_{\rho i}\left.\frac{\partial\rho}{\partial n_B}\right|_\chi + g_{\phi i}\left.\frac{\partial\phi}{\partial n_B}\right|_\chi. \tag{56}$$

Each of these partial derivatives of the vector meson fields can be found by differentiating their mean field equations of motion, resulting in a system of linear equations for $\partial\omega/\partial n_B$ and $\partial\rho/\partial n_B$ (and $\partial\phi/\partial n_B$) due to the $\Lambda_\omega g^2_\rho g^2_\omega \omega^2\rho^2$ coupling term. In principle, this system of linear equations as written below can be solved exactly, though in our work we solve them numerically:

$$\begin{aligned}
\sum_i g_{\phi i}x_i &= m^2_\phi\frac{\partial\phi}{\partial n_B},\\
\sum_i g_{\omega i}x_i &= m^2_\omega\frac{\partial\omega}{\partial n_B} + \frac{\xi}{2!}g^2_{\omega N}\omega^2\frac{\partial\omega}{\partial n_B}\\
&\quad + 2\Lambda_v g^2_{\rho N}g^2_{\omega N}\left(2\rho\frac{\partial\rho}{\partial n_B}\omega + \rho^2\frac{\partial\omega}{\partial n_B}\right),\\
\sum_i g_{\rho i}I_{3i}x_i &= m^2_\rho\frac{\partial\rho}{\partial n_B}\\
&\quad + 2\Lambda_v g^2_{\rho N}g^2_{\omega N}\left(\frac{\partial\rho}{\partial n_B}\omega^2 + 2\rho\omega\frac{\partial\omega}{\partial n_B}\right).
\end{aligned} \tag{57}$$

C. DDRMF model modifications

For the DDRMF models, as the coupling constants are density dependent, the contribution to the partial derivative of

the effective mass are given by

$$\left.\frac{\partial m_i^*}{\partial n_B}\right|_\chi = -\left.\frac{\partial g_{\sigma i}}{\partial n_B}\right|_\chi \sigma - g_{\sigma i}\left.\frac{\partial \sigma}{\partial n_B}\right|_\chi - \left.\frac{\partial g_{\xi i}}{\partial n_B}\right|_\chi \xi \tag{58}$$

$$- g_{\xi i}\left.\frac{\partial \xi}{\partial n_B}\right|_\chi - \left.\frac{\partial g_{\delta i}}{\partial n_B}\right|_\chi \delta - g_{\delta i}\left.\frac{\partial \delta}{\partial n_B}\right|_\chi \tag{59}$$

and the partial derivative of the mesonic contribution to the baryon chemical potential are given by

$$\left.\frac{\partial \mu_i^{(m)}}{\partial n_B}\right|_\chi = \left.\frac{\partial g_{\omega i}}{\partial n_B}\right|_\chi \omega + g_{\omega i}\left.\frac{\partial \omega}{\partial n_B}\right|_\chi + I_{3i}\left.\frac{\partial g_{\rho i}}{\partial n_B}\right|_\chi \rho \tag{60}$$

$$+ I_{3i} g_{\rho i}\left.\frac{\partial \rho}{\partial n_B}\right|_\chi + \left.\frac{\partial g_{\phi i}}{\partial n_B}\right|_\chi \phi + g_{\phi i}\left.\frac{\partial \phi}{\partial n_B}\right|_\chi, \tag{61}$$

where as usual, the partial derivatives with respect to n_B are taken at fixed composition. The mesonic equations of motion are likewise modified, though the overall structure of the resulting equations, and hence the solution methods, are no more complicated than for the NLRMF models.

The additional rearrangement term Σ^r can be differentiated in a similar manner. However, we note that in our context we are ultimately interested in $\tilde{\mu}_i$, which by its dependence on the difference of the neutron and baryon chemical potentials [as in Eq. (8)] leads to the contributions from $\partial\Sigma^r/\partial n_B$ from the neutron and ith baryon canceling each other out and ultimately does not contribute to $c_s^2 - c_e^2$.

VI. RESULTS

The sound speed differences for the models considered in this work are collected in the panels of Fig. 6. A common observation is that the sound speed difference experiences a sharp rise when a new species threshold is breached, due to a drop in c_e^2. This effect is quite dramatic for hyperons, particularly the Λ^0. The gradual decrease of the sound speed difference between consecutive species thresholds signifies that the system has returned to chemical and mechanical equilibrium. A comparison to $npe\mu$ matter alone highlights the remarkable effect of hyperons on the sound speed difference. Muons, due to their relatively small fraction compared to hyperons (see Fig. 1), do not impact the sound speed as much as hyperons. From the hyperon species, the Λ has the largest relative effect due to its population fraction.

There are more subtle differences, as reflected in μ^*, between the various models as well, due to variations in the baryon-meson and meson-meson interactions in the Lagrangian, the nature of the coupling constants (density dependent or not), as well as the recipe chosen to fix meson-hyperon couplings.

The implication of these trends in the sound speed difference is that the g-mode frequency, through the Brunt-Väisälä frequency, would be expected to manifest similar dramatic features for $npe\mu Y$ compositions. To compute the global g-mode frequency, we solve the linear perturbation equations (5) numerically by employing a fourth-order Runge-Kutta scheme to find the eigenvalue for ω obtained by subjecting this system of equations to the boundary conditions for the relativistic case outlined above Eqs. (5). In general, our integration procedure beginning at the starting point ($r = 0$) cannot know about the boundary condition at the surface ($r = R$) for arbitrary values of ω. However, the eigenvalue by definition is the value that satisfies both boundary conditions. Therefore, we perform a scan in frequency space (typically 10 to 1000 Hz) and perform the numerical integration repeatedly until we find the frequency for which both boundary conditions are simultaneously satisfied. This "shooting method" is the most common method employed in the literature on g-mode oscillations, and although other numerical methods are known in the literature, the shooting method is best suited to our goal of efficiently finding the principal eigenvalue. Since the solution set comprises overtones, we selected the lowest order g mode (highest frequency) by checking that the radial eigenfunction ξ_r has only one node inside the star. The corresponding eigenfrequency ω is plotted in the figures that follow. Indeed, our results for the g-mode oscillation frequency presented in Fig. 7, where the linear g-mode frequency $\nu = \omega/2\pi$ is plotted, demonstrates this fact. Specifically, a comparison of Figs. 4(a) and 4(b) for $npe\mu$ compositions and $npe\mu Y$ respectively (for each of the six RMF models used in this work), shows that in all but one of the $npe\mu Y$ models (GM1-Y5) a dramatically sharp increase in the oscillation frequency occurs at around 1.5–1.6 $M_\odot$. This corresponds to the lightest hyperon threshold, the lowest central density such that the first hyperonic species emerges, in the star. The g-mode frequencies for the stars with $npe\mu Y$ composition are approximately 350–750 Hz larger, depending on the stellar mass, than for those with $npe\mu$ composition. The case of GM1-Y5 is markedly different due to the absence of quartic interactions or SU(6) coupling constants, pushing the threshold density of hyperons near the tail end of the mass-radius curve. This qualitative behavior of the g-mode frequency upon the onset of new degrees of freedom is similar to results in [31,45,52], where a transition to quark matter in the form of a mixed/crossover quark matter phase was considered. In that case, the principal core g-mode frequency for hybrid stars containing quark matter was in the range ≈200–600 Hz, and therefore less dramatic than the the effect of hyperons. Since the frequencies of stars without strangeness degrees of freedom are only about 100—200 Hz, we conclude that a precise determination of the g-mode frequency, if and when observed in perturbed neutron stars, could potentially be a signature of strangeness, but also allow us to discern if such strangeness is bound (hyperons) or free (quarks).

VII. CONCLUSIONS

The main objective of this work was to ascertain the characteristics of g-mode oscillations of hyperonic stars, comparing them to the standard $npe\mu$ composition of a neutron star. Toward this end, we used a variety of relativistic mean field approaches to model the core of the star, where hyperons can be present. In particular, we used models GM1-Y5 [8,58], Big Apple [59,60], Hornick 65, 70 [61], DD-MEX [4,5,9,62], and DD-ME2 [4,5,9,63]. The models were chosen to sample a variety of different possible baryon-meson and meson-meson interactions as well as include different treatments of the

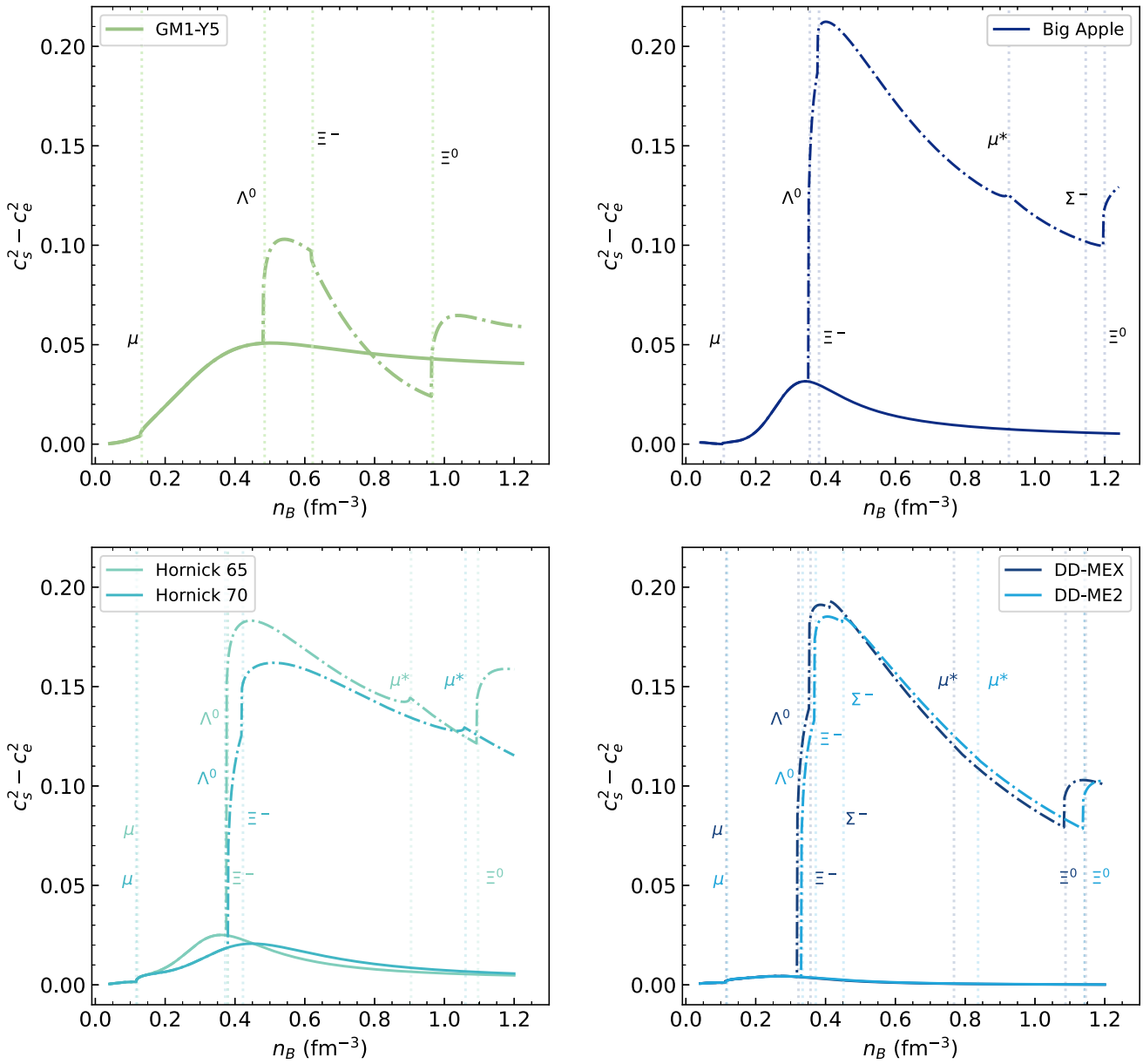

FIG. 6. Sound speed difference $c_s^2 - c_e^2$ plotted for the various models with $npe\mu$ matter in the dashed lines and $npe\mu Y$ matter in the dot-dashed lines. The vertical dotted lines represent the values of n_B at which new particles emerge corresponding to the "kinks" observed in the various curves, except for μ^* which instead denotes the locations where the muon vanishes. In all models, $c_s^2 - c_e^2$ exhibits a sharp rise upon the emergence of new particles, after which $c_s^2 - c_e^2$ begins to decrease until the arrival of a new particle. The appearance of hyperons generally appears to dramatically increase $c_s^2 - c_e^2$.

coupling constants, including models where the coupling constants vary with total baryon number density (DDRMF). All models satisfy current astrophysical constraints, producing equations of state stiff enough to produce maximally sized stars as well as constraints on the mass-radius relations in agreement with NICER constraints on PSR J0030 + 0451 and PSR J0740 + 6620. The calculated tidal deformabilities also agree with current constraints placed by GW170817.

While M-R curves only depend on the pressure vs density relation (EOS), the analysis of g-mode oscillations requires simultaneous information about the equilibrium and adiabatic squared sound speeds, $c_e^2 = dp/d\varepsilon$ and $c_s^2 = \partial p/\partial\varepsilon|_x$, where x are the local, independent composition variables. The distinction between these two sound speeds plays a central role in determining the Brunt-Väisälä frequencies $\omega^2 \propto c_e^{-2} - c_s^{-2}$ of nonradial g-mode oscillations. We generalized the method applied in [45,54] for $npe\mu$ matter to calculate the sound speed difference $c_s^2 - c_e^2$ from partial derivatives of linear combinations of chemical potentials, and applied this to obtain the g-mode spectrum for hyperonic stars described by relativistic mean field models.

We find that the g mode is sensitive to the presence of hyperons in neutron stars, as signalled by the sharp changes in sound speed difference at the lightest hyperon threshold

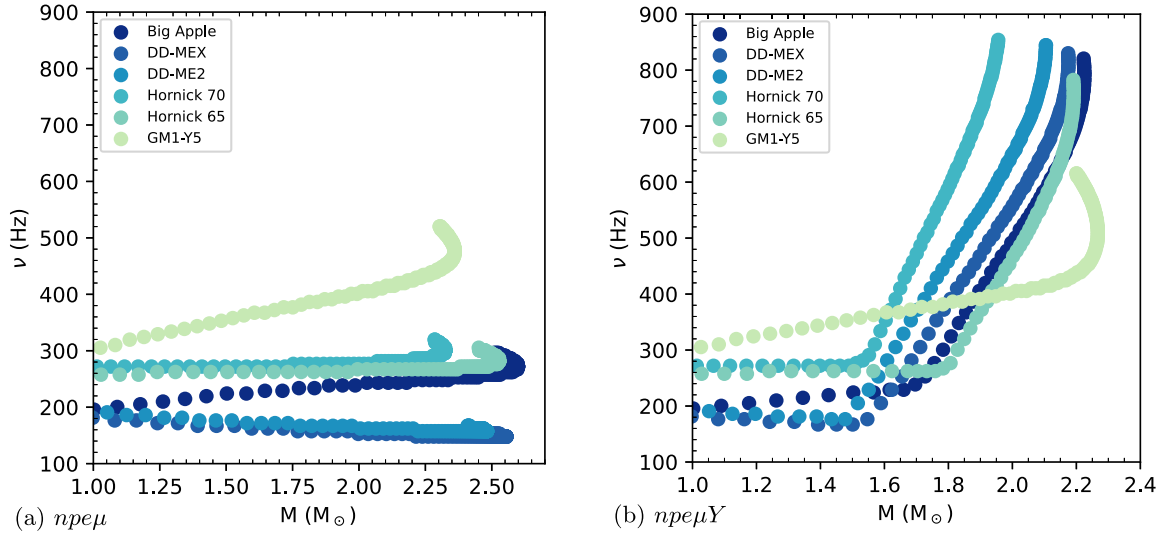

FIG. 7. g-mode oscillation frequency as a function of stellar mass for $npe\mu$ composition on the left and $npe\mu Y$ composition on the right. As a result of dependence of the sound speed difference on the number of equilibrating species in the system, the g-mode frequency rises sharply when the threshold density for a new species that participates in β-equilibrium reactions is breached. The case of GM1-Y5 is markedly different from the other models: the difference arises due to the absence of quartic interactions or SU(6) coupling constants, which forces hyperons to appear only at the tail end of the mass-radius curve.

(Fig. 6), raising the local Brunt-Väisälä frequency and the fundamental g-mode frequency of the star (Fig. 7). Contrasts of g-mode frequencies between normal and hyperonic stars containing quark matter (Fig. 7) form the principal results of our work. This contrast is a common feature that arises across the different models of hyperonic matter, and gives confidence that the effect is representative of the change in composition rather than an artifact of a specific model.

We briefly comment on two additional effects that can affect the g mode. Superfluidity/superconductivity introduces an additional flow component of the baryonic fluids leading to a new set of superfluid g modes which were discussed in some recent works [71]. The frequency of these superfluid modes can be quite large ($\approx$700 Hz) but they are strongly temperature dependent, unlike the normal fluid g modes considered here. The effect of magnetic field on the g mode is an interesting question that has yet to be investigated in detail, barring a few studies for the neutron star ocean [72]. It is possible that the magnetic field plays a role in core g modes if the field value is sufficiently large to change the composition from the zero field case.

The novel feature of this work is the first calculation of the two sound speeds in hyperonic matter and its impact on the principal g-mode frequency of hyperonic stars. Our results suggests that determining the composition of the star through g modes is a possible resolution to breaking degeneracies in inferences on the equation of state from M-R data alone and ascertaining if strangeness exists in neutron stars. Future work is aimed at quantifying the g-mode frequencies for hyperonic stars with a phase transition to quark matter or crossover transitions as in quarkyonic matter. It would also be interesting to study the evolution of the g mode in binary mergers where one or both components may be a hyperonic star, since such modes can be excited during inspiral and potentially alter the phase and amplitude of the gravitational wave signal from coalescing ordinary neutron stars.

ACKNOWLEDGMENTS

V.T. and P.J. are supported by the US National Science Foundation Grant No. PHY-2310003. V.T. would like to acknowledge support from the Richard D. Green Graduate Research Fellowship from the College of Natural Sciences and Mathematics at CSULB. The authors thank the International Centre for Theoretical Sciences (ICTS), Bangalore, India for organizing the online program Virtual Meeting on Compact Stars and QCD 2020 (code ICTS/csqcd2020/08), whereby this work was initiated.

APPENDIX A: DEMONSTRATING VALIDITY OF SOUND SPEED DIFFERENCE EXPRESSION

It was shown in [45] that from the definitions of c_s^2 and c_e^2 the sound speed difference $c_s^2 - c_e^2$ could be rewritten as

$$c_s^2 - c_e^2 = \frac{1}{\mu_{\rm avg}} \frac{\partial p}{\partial n_B}\bigg|_\chi - \frac{1}{\mu_n} \frac{dp}{dn_B}, \tag{A1}$$

where $\mu_{\rm avg} := \sum_i \mu_i x_i$, μ_n is the neutron chemical potential and $\partial p/\partial n_B|_\chi$ is the partial derivative of pressure with respect to baryon density n_B while holding composition fixed. This expression was then shown to be rewritable in terms of partial derivatives of $\tilde{\mu}_i$ for the specific case of npe and $npe\mu$ matter where the independent variables chosen were the electron fraction x_e in the first case and the lepton fraction x and muon fraction y in the second case. Then the sound speed difference

in the $npe\mu$ case was rewritable as

$$c_s^2 - c_e^2 = -\frac{n_B^2}{\mu_n}\left(\frac{\partial\tilde{\mu}_x}{\partial n_B}\bigg|_{x,y}\frac{dx}{dn_B} + \frac{\partial\tilde{\mu}_y}{\partial n_B}\bigg|_{x,y}\frac{dy}{dn_B}\right). \tag{A2}$$

Here, following the same steps outlined in [45], we can generalize these results to any arbitrary composition of baryons and leptons to get the expression shown in Eq. (7) starting from Eq. (A1).

We can start by taking the neutron fraction x_n and the electron fraction x_e to be the dependent fractions for all compositions. This then implies that all other baryon and lepton fractions are independent variables in our system. This type of scheme has the advantage of allowing us to write a generalized expression for sound speed difference for a variety of different compositions that may occur as n_B increases, and heavier particles such as hyperons appear without having to redefine and resolve for different independent and dependent fractions.

Then the pressure $p = p(n_B, x_1, \ldots, x_n)$ is a function of total baryon density n_B and the independent baryon, lepton fractions $x_1, \ldots, x_n$, so the total derivative of p with respect to n_B is given by

$$\frac{dp}{dn_B} = \frac{\partial p}{\partial n_B}\bigg|_{\chi} + \sum_i \frac{\partial p}{\partial x_i}\bigg|_{n_B, x_j\neq x_i}\frac{dx_i}{dn_B}, \tag{A3}$$

where the sum over i is over all independent baryon and lepton fractions/particles. When inserted into Eq. (A1) we can expand and collect terms in the following manner:

$$c_s^2 - c_e^2 = \left(\frac{1}{\mu_{\rm avg}} - \frac{1}{\mu_n}\right)\frac{\partial p}{\partial n_B}\bigg|_{n_B, x_j\neq x_i} \tag{A4}$$

$$-\frac{1}{\mu_n}\sum_i\left(\frac{\partial p}{\partial x_i}\bigg|_{n_B, x_j\neq x_i}\frac{dx_i}{dn_B}\right) \tag{A5}$$

$$= \left(\frac{\mu_n - \mu_{\rm avg}}{\mu_{\rm avg}\cdot\mu_n}\right)\frac{\partial p}{\partial n_B}\bigg|_{\chi} \tag{A6}$$

$$-\frac{1}{\mu_n}\sum_i\left(\frac{\partial p}{\partial x_i}\bigg|_{n_B, x_j\neq x_i}\frac{dx_i}{dn_B}\right). \tag{A7}$$

Next, the average chemical potential $\mu_{\rm avg}$ can be expanded as

$$\mu_{\rm avg} := \sum_j \mu_j x_j \tag{A8}$$

$$= x_n\mu_n + x_e\mu_e + \sum_i x_i\mu_i, \quad i \in \text{ind. var.} \tag{A9}$$

But with the neutron and electron fractions as dependent variables, we can rewrite them in terms of the other independent fractions using the constraints of charge neutrality and baryon number conservation:

$$1 = x_n + \sum_b x_b, \quad b \in \text{baryon}, \tag{A10}$$

$$0 = -x_e - x_\mu + \sum_b q_b x_b. \tag{A11}$$

After solving for x_n and x_e in terms of the other fractions, using these two constraints $\mu_{\rm avg}$ becomes

$$\mu_{\rm avg} = \left(1 - \sum_b x_b\right)\mu_n + \left(-x_\mu + \sum_b q_b x_b\right)\mu_e \tag{A12}$$

$$+ x_\mu\mu_\mu + \sum_b x_b\mu_b. \tag{A13}$$

Then the difference $\mu_n - \mu_{\rm avg}$ becomes

$$\mu_n - \mu_{\rm avg} = \sum_b x_b\mu_n - \sum_b x_b\mu_b - \sum_b q_b x_b\mu_e \tag{A14}$$

$$+ x_\mu(\mu_e - \mu_\mu) \tag{A15}$$

$$= \sum_b(\mu_n - q_b\mu_e - \mu_b)x_b \tag{A16}$$

$$+ x_\mu(\mu_e - \mu_\mu). \tag{A17}$$

But we see that the terms inside of the parentheses are exactly combinations of chemical potentials that vanish in β equilibrium,

$$\tilde{\mu}_b = \mu_n - q_b\mu_e - \mu_b = 0, \tag{A18}$$

$$\tilde{\mu}_\mu = \mu_e - \mu_\mu, \tag{A19}$$

which allows us to rewrite $\mu_{\rm avg}$ in a concise manner in terms of $\tilde{\mu}_i$:

$$\mu_n - \mu_{\rm avg} = \sum_b \tilde{\mu}_b x_b + \tilde{\mu}_\mu x_\mu \tag{A20}$$

$$= \sum_i \tilde{\mu}_i x_i, \quad i \in \text{all ind. vars.} \tag{A21}$$

The remaining steps follow in a similar fashion as described in [45]. In β equilibrium $\mu_n - \mu_{\rm avg}$ is zero since $\tilde{\mu}_i = 0$ for all i. The sound speed difference expression reduces to

$$c_s^2 - c_e^2 = -\frac{1}{\mu_n}\sum_i \frac{\partial p}{\partial x_i}\bigg|_{n_B, x_j\neq x_i}\frac{dx_i}{dn_B}. \tag{A22}$$

Using $p = n_B^2\partial E/\partial n_B|_\chi$ we can rewrite this as

$$c_s^2 - c_e^2 = -\frac{n_B^2}{\mu_n}\sum_i \frac{\partial E}{\partial x_i}\bigg|_{n_B, x_j\neq x_i}\frac{dx_i}{dn_B} \tag{A23}$$

$$= \frac{n_B^2}{\mu_n}\sum_i \frac{\partial\tilde{\mu}_i}{\partial n_B}\bigg|_{\chi}\frac{dx_i}{dn_B}, \tag{A24}$$

where Eq. (A24) is the expression we use in calculating the sound speed difference in this paper.

APPENDIX B: MESONIC MEAN FIELD EQUATIONS

The forms of the Euler-Lagrange field equations for the mesons as specified for the general Lagrangian used in our work, that is, including the form of the meson-meson

interactions as given in Eq. (19), are

$$m_\sigma^2\sigma + bg_{\sigma N}^3\sigma^2 + cg_{\sigma N}^4\sigma^3 = \sum_i g_{\sigma i}n_i^s, \quad \text{(B1)}$$

$$m_\omega^2\omega + \frac{\xi}{3!}g_{\omega N}^2\omega^3 + 2\Lambda_\omega g_{\rho N}^2 g_{\omega N}^2\rho^2\omega = \sum_i g_{\omega i}n_i, \quad \text{(B2)}$$

$$m_\rho^2\rho + 2\Lambda_\omega g_{\rho N}^2 g_{\omega N}^2\rho\omega^2 = \sum_i g_{\rho i}I_{3i}n_i, \quad \text{(B3)}$$

$$m_\phi^2\phi = \sum_i g_{\phi i}n_i, \quad \text{(B4)}$$

$$m_\xi^2\xi = \sum_i g_{\xi i}n_i^s, \quad \text{(B5)}$$

$$m_\delta^2\delta = \sum_i I_{3i}g_{\delta i}n_i^s. \quad \text{(B6)}$$

[1] T. Zhao and J. M. Lattimer, Quarkyonic matter equation of state in beta-equilibrium, Phys. Rev. D **102**, 023021 (2020).

[2] T. Demircik, C. Ecker, and M. Järvinen, Dense and Hot QCD at Strong Coupling, Phys. Rev. X **12**, 041012 (2022).

[3] V. Dexheimer, K. Aryal, C. Constantinou, J. Peterson, and R. L. S. Farias, 3-dimensional QCD phase diagrams for strange matter, J. Phys. Conf. Ser. **1602**, 012013 (2020).

[4] K. Huang, J. Hu, Y. Zhang, and H. Shen, The possibility of the secondary object in GW190814 as a neutron star, Astrophys. J. **904**, 39 (2020).

[5] V. B. Thapa, A. Kumar, and M. Sinha, Baryonic dense matter in view of gravitational-wave observations, Mon. Not. R. Astron. Soc. **507**, 2991 (2021).

[6] A. Clevinger, J. Corkish, K. Aryal, and V. Dexheimer, Hybrid equations of state for neutron stars with hyperons and deltas, Eur. Phys. J. A **58**, 96 (2022).

[7] N. K. Glendenning, Neutron stars are giant hypernuclei? Astrophys. J. **293**, 470 (1985).

[8] N. K. Glendenning and S. A. Moszkowski, Reconciliation of Neutron-Star Masses and Binding of the Λ in Hypernuclei, Phys. Rev. Lett. **67**, 2414 (1991).

[9] Z.-H. Tu and S.-G. Zhou, Effects of the ϕ meson on the properties of hyperon stars in the density-dependent relativistic mean field model, Astrophys. J. **925**, 16 (2022).

[10] V. Dexheimer, R. O. Gomes, T. Klähn, S. Han, and M. Salinas, GW190814 as a massive rapidly rotating neutron star with exotic degrees of freedom, Phys. Rev. C **103**, 025808 (2021).

[11] V. Dexheimer, K. D. Marquez, and D. P. Menezes, Delta baryons in neutron-star matter under strong magnetic fields, Eur. Phys. J. A **57**, 216 (2021).

[12] D. Chatterjee and I. Vidaña, Do hyperons exist in the interior of neutron stars? Eur. Phys. J. A **52**, 29 (2016).

[13] R. W. Romani, D. Kandel, A. V. Filippenko, T. G. Brink, and W. Zheng, PSR J0952-0607: The fastest and heaviest known galactic neutron star, Astrophys. J. Lett. **934**, L17 (2022).

[14] R. Abbott *et al.*, GW190814: Gravitational waves from the coalescence of a 23 solar mass black hole with a 2.6 solar mass compact object, Astrophys. J. Lett. **896**, L44 (2020).

[15] I. Bombaci, The hyperon puzzle in neutron stars, in Proceedings of the 12th International Conference on Hypernuclear and Strange Particle Physics (HYP2015), JPS Conf. Proc. **17**, 101002 (2017)].

[16] E. E. Kolomeitsev, K. A. Maslov, and D. N. Voskresensky, Hyperon puzzle and the RMF model with scaled hadron masses and coupling constants, J. Phys.: Conf. Ser. **668**, 012064 (2016).

[17] B. K. Pradhan and D. Chatterjee, Effect of hyperons on f-mode oscillations in neutron stars, Phys. Rev. C **103**, 035810 (2021).

[18] T. E. Riley, A. L. Watts, S. Bogdanov, P. S. Ray, R. M. Ludlam, S. Guillot, Z. Arzoumanian, C. L. Baker, A. V. Bilous, D. Chakrabarty, K. C. Gendreau, A. K. Harding, W. C. G. Ho, J. M. Lattimer, S. M. Morsink, and T. E. Strohmayer, A NICER view of PSR J0030 + 0451: Millisecond pulsar parameter estimation, Astrophys. J. **887**, L21 (2019).

[19] M. C. Miller, F. K. Lamb, A. J. Dittmann, S. Bogdanov, Z. Arzoumanian, K. C. Gendreau, S. Guillot, A. K. Harding, W. C. G. Ho, J. M. Lattimer, R. M. Ludlam, S. Mahmoodifar, S. M. Morsink, P. S. Ray, T. E. Strohmayer, K. S. Wood, T. Enoto, R. Foster, T. Okajima, G. Prigozhin, and Y. Soong, PSR J0030 + 0451 mass and radius from nicer data and implications for the properties of neutron star matter, Astrophys. J. **887**, L24 (2019).

[20] M. C. Miller, F. K. Lamb, A. J. Dittmann, S. Bogdanov, Z. Arzoumanian, K. C. Gendreau, S. Guillot, W. C. G. Ho, J. M. Lattimer, M. Loewenstein, S. M. Morsink, P. S. Ray, M. T. Wolff, C. L. Baker, T. Cazeau, S. Manthripragada, C. B. Markwardt, T. Okajima, S. Pollard, I. Cognard, H. T. Cromartie, E. Fonseca, L. Guillemot, M. Kerr, A. Parthasarathy, T. T. Pennucci, S. Ransom, and I. Stairs, The radius of J0740 + 6620 from NICER and XMM-Newton data, Astrophys. J. Lett. **918**, L28 (2021).

[21] T. E. Riley, A. L. Watts, P. S. Ray, S. Bogdanov, S. Guillot, S. M. Morsink, A. V. Bilous, Z. Arzoumanian, D. Choudhury, J. S. Deneva, K. C. Gendreau, A. K. Harding, W. C. G. Ho, J. M. Lattimer, M. Loewenstein, R. M. Ludlam, C. B. Markwardt, T. Okajima, C. Prescod-Weinstein, R. A. Remillard, M. T. Wolff, E. Fonseca, H. T. Cromartie, M. Kerr, T. T. Pennucci, A. Parthasarathy, S. Ransom, I. Stairs, L. Guillemot, and I. Cognard, A NICER view of the massive pulsar PSR J0740 + 6620 informed by radio timing and XMM-Newton spectroscopy, Astrophys. J. Lett. **918**, L27 (2021).

[22] B. P. Abbott (LIGO Scientific Collaboration and Virgo Collaboration), GW170817: Observation of Gravitational Waves from a Binary Neutron Star Inspiral, Phys. Rev. Lett. **119**, 161101 (2017).

[23] L. Baiotti, Gravitational waves from neutron star mergers and their relation to the nuclear equation of state, Prog. Part. Nucl. Phys. **109**, 103714 (2019).

[24] W. Wei, B. Irving, M. Salinas, T. Klähn, and P. Jaikumar, Camouflage of the phase transition to quark matter in neutron stars, Astrophys. J. **887**, 151 (2019).

[25] W. Wei, M. Salinas, T. Klähn, P. Jaikumar, and M. Barry, Lifting the veil on quark matter in compact stars with core g-mode oscillations, Astrophys. J. **904**, 187 (2020).

[26] M. Alford, M. Braby, M. Paris, and S. Reddy, Hybrid stars that masquerade as neutron stars, Astrophys. J. **629**, 969 (2005).

[27] S. Ghosh, B. K. Pradhan, D. Chatterjee, and J. Schaffner-Bielich, Multi-physics constraints at different densities to probe nuclear symmetry energy in hyperonic neutron stars, Front. Astron. Space Sci. **9**, 864294 (2022).

[28] I. Vidaña, Hyperons: The strange ingredients of the nuclear equation of state, Proc. R. Soc. A. **474**, 20180145 (2018).

[29] P. F. Bedaque and A. W. Steiner, Hypernuclei and the hyperon problem in neutron stars, Phys. Rev. C **92**, 025803 (2015).

[30] H. R. Fu, J. J. Li, A. Sedrakian, and F. Weber, Massive relativistic compact stars from SU(3) symmetric quark models, Phys. Lett. B **834**, 137470 (2022).

[31] C. Constantinou, S. Han, P. Jaikumar, and M. Prakash, g modes of neutron stars with hadron-to-quark crossover transitions, Phys. Rev. D **104**, 123032 (2021).

[32] L. Tolos, M. Centelles, and A. Ramos, Equation of state for nucleonic and hyperonic neutron stars with mass and radius constraints, Astrophys. J. **834**, 3 (2017).

[33] T. G. Cowling, The non-radial oscillations of polytropic stars, Mon. Not. R. Astron. Soc. **101**, 367 (1941).

[34] K. D. Kokkotas and B. G. Schmidt, Quasinormal modes of stars and black holes, Living Rev. Relativ. **2**, 2 (1999).

[35] K. S. Thorne and A. Campolattaro, Non-radial pulsation of general-relativistic stellar models. I. Analytic analysis for L >= 2, Astrophys. J. **149**, 591 (1967).

[36] K. D. Kokkotas, T. A. Apostolatos, and N. Andersson, The inverse problem for pulsating neutron stars: A 'fingerprint analysis' for the supranuclear equation of state, Mon. Not. R. Astron. Soc. **320**, 307 (2001).

[37] N. Stergioulas, A. Bauswein, K. Zagkouris, and H.-T. Janka, Gravitational waves and non-axisymmetric oscillation modes in mergers of compact object binaries, Mon. Not. R. Astron. Soc. **418**, 427 (2011).

[38] S. Vretinaris, N. Stergioulas, and A. Bauswein, Empirical relations for gravitational-wave asteroseismology of binary neutron star mergers, Phys. Rev. D **101**, 084039 (2020).

[39] C. Chirenti, R. Gold, and M. C. Miller, Gravitational waves from F-modes excited by the inspiral of highly eccentric neutron star binaries, Astrophys. J. **837**, 67 (2017).

[40] J. Steinhoff, T. Hinderer, T. Dietrich, and F. Foucart, Spin effects on neutron star fundamental-mode dynamical tides: Phenomenology and comparison to numerical simulations, Phys. Rev. Res. **3**, 033129 (2021).

[41] T. K. Chan, Y.-H. Sham, P. T. Leung, and L.-M. Lin, Multipolar universal relations between f-mode frequency and tidal deformability of compact stars, Phys. Rev. D **90**, 124023 (2014).

[42] T. Hinderer, A. Taracchini, F. Foucart, A. Buonanno, J. Steinhoff, M. Duez, L. E. Kidder, H. P. Pfeiffer, M. A. Scheel, B. Szilagyi, K. Hotokezaka, K. Kyutoku, M. Shibata, and C. W. Carpenter, Effects of Neutron-Star Dynamic Tides on Gravitational Waveforms within the Effective-One-Body Approach, Phys. Rev. Lett. **116**, 181101 (2016).

[43] G. Pratten, P. Schmidt, and T. Hinderer, Gravitational-wave asteroseismology with fundamental modes from compact binary inspirals, Nat. Commun. **11**, 2553 (2020).

[44] W. C. G. Ho, D. I. Jones, N. Andersson, and C. M. Espinoza, Gravitational waves from transient neutron star f-mode oscillations, Phys. Rev. D **101**, 103009 (2020).

[45] P. Jaikumar, A. Semposki, M. Prakash, and C. Constantinou, g-mode oscillations in hybrid stars: A tale of two sounds, Phys. Rev. D **103**, 123009 (2021).

[46] J. D. Walecka, A theory of highly condensed matter, Ann. Phys. (NY) **83**, 491 (1974).

[47] N. K. Glendenning, *Compact Stars* (Springer, New York, 1997).

[48] E. M. Kantor and M. E. Gusakov, Composition temperature-dependent g modes in superfluid neutron stars, Mon. Not. R. Astron. Soc. Lett. **442**, L90 (2014).

[49] A. Reisenegger and P. Goldreich, A new class of g-modes in neutron stars, Astrophys. J. **395**, 240 (1992).

[50] P. N. McDermott, H. M. van Horn, and J. F. Scholl, Nonradial g-mode oscillations of warm neutron stars, Astrophys. J. **268**, 837 (1983).

[51] T. G. Cowling, The theory of stellar structure, 1932–1942, Observatory **64**, 224 (1942).

[52] T. Zhao, C. Constantinou, P. Jaikumar, and M. Prakash, Quasinormal g modes of neutron stars with quarks, Phys. Rev. D **105**, 103025 (2022).

[53] D. Lai, Secular instability of g modes in rotating neutron stars, Mon. Not. R. Astron. Soc. **307**, 1001 (1999).

[54] D. Lai, Resonant oscillations and tidal heating in coalescing binary neutron stars, Mon. Not. R. Astron. Soc. **270**, 611 (1994).

[55] T. Zhao and J. M. Lattimer, Universal relations for neutron star f-mode and g-mode oscillations, Phys. Rev. D **106**, 123002 (2022).

[56] S. Han, M. A. A. Mamun, S. Lalit, C. Constantinou, and M. Prakash, Treating quarks within neutron stars, Phys. Rev. D **100**, 103022 (2019).

[57] M. Oertel, M. Hempel, T. Klähn, and S. Typel, Equations of state for supernovae and compact stars, Rev. Mod. Phys. **89**, 015007 (2017).

[58] M. Oertel, C. Providência, F. Gulminelli, and A. R. Raduta, Hyperons in neutron star matter within relativistic mean-field models, J. Phys. G: Nucl. Part. Phys. **42**, 075202 (2015).

[59] F. J. Fattoyev, C. J. Horowitz, J. Piekarewicz, and B. Reed, GW190814: Impact of a 2.6 solar mass neutron star on the nucleonic equations of state, Phys. Rev. C **102**, 065805 (2020).

[60] H. C. Das, A. Kumar, B. Kumar, S. K. Biswal, and S. K. Patra, BigApple force and its implications to finite nuclei and astrophysical objects, Int. J. Mod. Phys. E **30**, 2150088 (2021).

[61] N. Hornick, L. Tolos, A. Zacchi, J.-E. Christian, and J. Schaffner-Bielich, Relativistic parameterizations of neutron matter and implications for neutron stars, Phys. Rev. C **98**, 065804 (2018).

[62] A. Taninah, S. Agbemava, A. Afanasjev, and P. Ring, Parametric correlations in energy density functionals, Phys. Lett. B **800**, 135065 (2020).

[63] G. A. Lalazissis, T. Nikšić, D. Vretenar, and P. Ring, New relativistic mean-field interaction with density-dependent meson-nucleon couplings, Phys. Rev. C **71**, 024312 (2005).

[64] B. K. Pradhan, D. Chatterjee, M. Lanoye, and P. Jaikumar, General relativistic treatment of f-mode oscillations of hyperonic stars, Phys. Rev. C **106**, 015805 (2022).

[65] T. Miyatsu, M.-K. Cheoun, and K. Saito, Equation of state for neutron stars in SU(3) flavor symmetry, Phys. Rev. C **88**, 015802 (2013).

[66] A. Schmitt, *Dense Matter in Compact Stars: A Pedagogical Introduction*, Lecture Notes in Physics, Vol. 811 (Springer, Heidelberg, 2010).

[67] J. Schaffner, C. B. Dover, A. Gal, C. Greiner, D. J. Millener, and H. Stocker, Multiply strange nuclear systems, Ann. Phys. (NY) **235**, 35 (1994).

[68] J. Schaffner-Bielich and A. Gal, Properties of strange hadronic matter in bulk and in finite systems, Phys. Rev. C **62**, 034311 (2000).

[69] I. A. Rather, U. Rahaman, V. Dexheimer, A. A. Usmani, and S. K. Patra, Heavy magnetic neutron stars, Astrophys. J. **917**, 46 (2021).

[70] T. Klähn, D. Blaschke, S. Typel, E. N. E. van Dalen, A. Faessler, C. Fuchs, T. Gaitanos, H. Grigorian, A. Ho, E. E. Kolomeitsev, M. C. Miller, G. Röpke, J. Trümper, D. N. Voskresensky, F. Weber, and H. H. Wolter, Constraints on the high-density nuclear equation of state from the phenomenology of compact stars and heavy-ion collisions, Phys. Rev. C **74**, 035802 (2006).

[71] V. A. Dommes and M. E. Gusakov, Oscillations of superfluid hyperon stars: Decoupling scheme and g-modes, Mon. Not. R. Astron. Soc. **455**, 2852 (2016).

[72] B. W. Carroll, E. G. Zweibel, C. J. Hansen, P. N. McDermott, M. P. Savedoff, J. H. Thomas, and H. M. van Horn, Oscillation spectra of neutron stars with strong magnetic fields, Astrophys. J. **305**, 767 (1986).